

Reduced basis approximation and *a posteriori* error estimation for Stress Intensity Factors: Application to Failure Analysis

D.B.P. HUYNH¹, J. PERAIRE^{1,3}, A.T. PATERA^{1,3} and G.R. LIU^{1,2}

¹Singapore-MIT Alliance

²National University of Singapore

³Massachusetts Institute of Technology

Abstract—This paper reports the development of reduced basis approximations, rigorous *a posteriori* error bounds, and offline-online computational procedures for the accurate, fast and reliable predictions of stress intensity factors or strain energy release rate for “Mode I” linear elastic crack problem. We demonstrate the efficiency and rigor of our numerical method in several examples. We apply our method to a practical failure design application.

Index Terms—reduced basis approximation, *a posteriori* error estimation, offline-online procedures, fracture mechanics, stress intensity factor, energy release rate, linear elasticity, finite element method, quadratic outputs.

I. INTRODUCTION

The stress intensity factor [18] is one of the most important quantities in Fracture Mechanics: it characterizes the stress, strain, and displacement fields in the near crack tip region. Stress intensity factor plays a dominant role in many fracture related problems. For example, in many failure design scenarios, we need to accurately evaluate stress intensity factors in order to determine several fracture parameters (for example, critical crack length, designed failure life of a component in the structural system, etc). In practical applications, we often require fast stress intensity factor calculations in order to produce satisfied evaluations in reasonable time. In short, in design new structures or assess the integrity of existing structures, the stress intensity factor (SIF) need to be computed repeatedly in real-time; and most importantly, the SIF must be accurate and reliable.

There are two main approaches to calculates the stress intensity factor: for simple problem we can either extract the SIF from reference handbook or database. For more complicated problems, however we need to directly compute the SIF numerically, which can be very time consuming.

Our goal is to develop a computational method that provides both *fast* and *reliable* prediction of stress intensity factors based on the reduced basis method [4], [2], [3], [5], [6], [7], [16], [20], [15]. The main ingredients of the reduced basis method are (i) reduced basis approximations [20], [15], [14] that provide rapid and uniform convergence; (ii) *a posteriori* error estimators [20] that provide sharp and rigorous bounds for the error in the output (here the SIF); and (iii) offline/online computational strategies [20], [15], [14], [21], [25]

that allow rapid calculation of both our output approximation and associated error bound.

We shall first describe our method, and then apply it to a particular fracture problem to demonstrate the advantages of our technique. The paper is organized as follows. In Section II we introduce first the standard problem statement and then an equivalent new formulation that enables us to extract our output – the stress intensity factor – as a “compliant” energy release rate. In Section III, we discuss the extended finite element method. In Section IV and Section V, we describe our reduced basis approximation and the associated *a posteriori* error estimation, which is particularly tailored to the stress intensity factor. In Section VI, we apply our results to one particular design problem to demonstrate the usefulness of our technique. And finally, in Section VII, we draw conclusions.

II. ABSTRACT STATEMENT

A. Classical Formulation

We consider a two-dimensional domain $\Omega \in \mathbb{R}^2$ with boundary $\partial\Omega$. We then introduce the Hilbert space

$$X = \{v \equiv (v_1, v_2) \in (H^1(\Omega))^2 | v_i = 0 \text{ on } \Gamma_D^i, i = 1, 2\}, \quad (1)$$

where $\Gamma_D^i \subset \partial\Omega$ is the part of $\partial\Omega$ on which we shall impose homogeneous Dirichlet (zero displacement) boundary conditions. Here $H^1(\Omega) = \{v \in L^2(\Omega) | \nabla v \in (L^2(\Omega))^2\}$ where $L^2(\Omega)$ is the space of square-integrable functions over Ω . We equip our space with inner product and associated norm $(\cdot, \cdot)_X$ and $\|\cdot\|_X = \sqrt{(\cdot, \cdot)_X}$, respectively.

We then define our parameter set $\mathcal{D} \in \mathbb{R}^P$, a typical point in which shall be denoted $\mu \equiv (\mu_1, \dots, \mu_P)$. The parameter describes the “input” for the problem, such as the physical properties or geometry of the model; in this paper, the number of “input” parameters, P will be 3. We further assume that the domain Ω contains a crack, and (for convenience) that μ_1 represents the crack length.

We next introduce the “exact” two-dimensional plane-strain linear elasticity model (extension to plane-stress is of course straightforward [18]). We shall denote dimensional quantities with a superscript \sim ; conversely, no superscript \sim implies a non-dimensional quantity. We scale the dimensional spatial coordinates \tilde{x} by a characteristic length \tilde{D} to obtain $x =$

$(x_1, x_2) \in \Omega$). We scale the dimensional displacement \tilde{u} by $D\tilde{\sigma}_0/\tilde{E}_{\text{crack}}$ to obtain $u = (u_1, u_2)$; here $\tilde{\sigma}_0$ is a characteristic (imposed farfield) stress, and \tilde{E}_{crack} is the Young's modulus of the material in the vicinity of the crack.

The displacement field $u(\mu) \in X$ satisfies the weak form

$$a(u(\mu), v; \mu) = f(v; \mu), \quad \forall v \in X; \quad (2)$$

here a is a parametrized bilinear form $a : X \times X \times \mathcal{D} \rightarrow \mathbb{R}$, and f is a parametrized linear form $f : X \times \mathcal{D} \rightarrow \mathbb{R}$. We assume that our bilinear form a is coercive, $a(w, w; \mu) \geq \alpha(\mu)\|w\|_X^2 \geq \alpha_0\|w\|_X^2$, $\forall w \in X$, $\forall \mu \in \mathcal{D}$, for some positive α_0 ; continuous, $a(w, v; \mu) \leq \gamma(\mu)\|w\|_X\|v\|_X \leq \gamma_0\|w\|_X\|v\|_X$, $\forall w, v \in X$, $\forall \mu \in \mathcal{D}$, for some finite γ_0 ; and symmetric, $a(w, v; \mu) = a(v, w; \mu)$, $\forall w, v \in X$. We also assume that our linear form f is bounded. Of course, a and f represent the standard linear elasticity weak form – particular instance of which we shall develop in the next section.

Moreover, we further require that $a(\cdot, \cdot; \mu)$ and $f(\cdot; \mu)$ are “affine” in the parameter that have the following forms

$$a(w, v; \mu) = \sum_{q=1}^{Q^a} \Theta_q^a(\mu) a_q(w, v), \quad (3)$$

$$f(v; \mu) = \sum_{q=1}^{Q^f} \Theta_q^f(\mu) f_q(v), \quad (4)$$

where $\Theta_q^a(\mu), \Theta_q^f(\mu) : \mathcal{D} \rightarrow \mathbb{R}$ and $a_q(w, v) : X \times X \rightarrow \mathbb{R}$, $f_q(v) : X \rightarrow \mathbb{R}$, are parameter-dependent functions and parameter-independent continuous bilinear/linear forms, respectively. We shall further assume that the functions $\Theta_q^a(\mu)$ and $\Theta_q^f(\mu)$ are smooth, $\Theta_q^a(\mu) \in \mathcal{C}^1(\mathcal{D})$, $1 \leq q \leq Q^a$ and $\Theta_q^f(\mu) \in \mathcal{C}^1(\mathcal{D})$, $1 \leq q \leq Q^f$, and that the a_q , $1 \leq q \leq Q^a$, are symmetric.

We next define our output of interest $G(\mu)$: the energy release rate as [22]

$$G(\mu) = -\frac{1}{2} \sum_{q=1}^{Q^a} \frac{\partial \Theta_q^a(\mu)}{\partial \mu_1} a_q(u(\mu), u(\mu)) + \sum_{q=1}^{Q^f} \frac{\partial \Theta_q^f(\mu)}{\partial \mu_1} f_q(u(\mu)), \quad (5)$$

where we recall that μ_1 is the component in μ that represents the crack length. Note the partial derivatives act only on the “explicit” μ dependence though the last arguments of a and f . We thus introduce a symmetric parametrized bilinear form $b : X \times X \times \mathcal{D}$ and a parametrized linear form $\ell : X \times \mathcal{D}$,

$$b(w, v; \mu) = -\frac{1}{2} \sum_{q=1}^{Q^a} \frac{\partial \Theta_q^a(\mu)}{\partial \mu_1} a_q(w, v), \quad (6)$$

$$\ell(v; \mu) = \sum_{q=1}^{Q^f} \frac{\partial \Theta_q^f(\mu)}{\partial \mu_1} f_q(v). \quad (7)$$

in terms of which our output can be expressed as $G(\mu) = b(u(\mu), u(\mu); \mu) + \ell(u(\mu); \mu)$. Note that the output $G(\mu)$ is the sum of a *quadratic* output and a “*non-compliant*” linear output.

Our abstract statement is then: for any $\mu \in \mathcal{D}$, find $G(\mu) \in \mathbb{R}$ given by

$$G(\mu) = b(u(\mu), u(\mu); \mu) + \ell(u(\mu); \mu), \quad (8)$$

where the displacement field $u(\mu) \in X$ satisfies the equilibrium equations (2). This problem statement focuses on the energy release rate; however we can also readily extract the stress intensity factor (SIF) as a “derived” output.

In this paper we shall restrict our attention exclusively to “Mode I,” or open-mode, fracture problems. It is known in fracture mechanics theory [18] that, for open-mode fracture problems, the non-dimensional stress intensity factor $K(\mu) = \tilde{K}(\mu)/(\tilde{\sigma}_0\sqrt{\tilde{D}})$ and energy release rate G are directly related as

$$K(\mu) = \sqrt{\frac{G(\mu)}{1 - \nu_{\text{crack}}^2}}, \quad \text{plane strain}, \quad (9)$$

where ν_{crack} is the Poisson ratio of the material in the vicinity of the crack.

B. Expanded Formulation

We consider the following system of equations

$$a(u(\mu), v; \mu) = f(v; \mu), \quad \forall v \in X, \quad (10)$$

$$a(z(\mu), v; \mu) = b(u(\mu), v; \mu) + \frac{1}{2}\ell(v; \mu), \quad \forall v \in X. \quad (11)$$

Note that z here is essentially the adjoint associated with our quadratic-linear output [13], [11].

Now we set

$$U_+(\mu) = \frac{1}{2}(u(\mu) + z(\mu)), \quad U_-(\mu) = \frac{1}{2}(u(\mu) - z(\mu)), \quad (12)$$

and define the parametrized symmetric bilinear form $\mathcal{A} : \mathcal{X} \times \mathcal{X} \times \mathcal{D} \rightarrow \mathbb{R}$ and parametrized linear form $\mathcal{F} : \mathcal{X} \times \mathcal{D} \rightarrow \mathbb{R}$ as

$$\begin{aligned} \mathcal{A}(\mathcal{W}, \mathcal{V}; \mu) &= -b(W_+, V_+; \mu) + 2a(W_+, V_+; \mu) - b(W_-, V_+; \mu) \\ &\quad - b(W_+, V_-; \mu) - b(W_-, V_-; \mu) - 2a(W_-, V_-; \mu), \\ \mathcal{F}(\mathcal{V}; \mu) &= f(V_+; \mu) + \frac{1}{2}\ell(V_+; \mu) - f(V_-; \mu) + \frac{1}{2}\ell(V_-; \mu), \end{aligned} \quad (13)$$

where $\mathcal{X} \equiv X \times X$, and $\mathcal{W} \equiv (U_+, U_-)$, $\mathcal{V} \equiv (V_+, V_-)$. We equip \mathcal{X} with inner product and associated norm $(\cdot, \cdot)_{\mathcal{X}}$ and $\|\cdot\|_{\mathcal{X}} = \sqrt{(\cdot, \cdot)_{\mathcal{X}}}$, respectively: our choice of $(\cdot, \cdot)_{\mathcal{X}}$ is $(\mathcal{W}, \mathcal{V})_{\mathcal{X}} = a(W_+, V_+; \bar{\mu}) + a(W_-, V_-; \bar{\mu})$, $\forall \mathcal{W}, \mathcal{V} \in \mathcal{X}$; here $\bar{\mu}$ is a particular parameter in \mathcal{D} .

It is observed that $\mathcal{F}(\mathcal{U}(\mu); \mu)$, $\mathcal{U} = (U_+, U_-)$, is equivalent to the energy release rate $G(\mu)$ in the “classical” formulation. We refer to [22] for a detailed proof of this equivalence.

Our abstract statement is thus: given $\mu \in \mathcal{D}$, find (the “compliant” output)

$$\mathcal{G}(\mu) = \mathcal{F}(\mathcal{U}(\mu); \mu), \quad (14)$$

where $\mathcal{U}(\mu) \in \mathcal{X}$ satisfies

$$\mathcal{A}(\mathcal{U}(\mu), \mathcal{V}; \mu) = \mathcal{F}(\mathcal{V}; \mu), \quad \forall \mathcal{V} \in \mathcal{X}; \quad (15)$$

here \mathcal{A} and \mathcal{F} are the “big” operators defined in (13).

We note that it directly follows from the definitions of \mathcal{A} and \mathcal{F} that both \mathcal{A} and \mathcal{F} are affine in the parameter. In particular,

$$\mathcal{A}(\mathcal{W}, \mathcal{V}; \mu) = \sum_{q=1}^{Q^{\mathcal{A}}} \Theta_q^{\mathcal{A}}(\mu) \mathcal{A}_q(\mathcal{W}, \mathcal{V}), \quad (16)$$

$$\mathcal{F}(\mathcal{V}; \mu) = \sum_{q=1}^{Q^{\mathcal{F}}} \Theta_q^{\mathcal{F}}(\mu) \mathcal{F}_q(\mathcal{V}), \quad (17)$$

where $\Theta_q^A : \mathcal{D} \rightarrow \mathbb{R}$, $\Theta_q^F : \mathcal{D} \rightarrow \mathbb{R}$, and $\mathcal{A}_q(\mathcal{W}, \mathcal{V}) : \mathcal{X} \times \mathcal{X} \rightarrow \mathbb{R}$, $\mathcal{F}_q(\mathcal{V}) : \mathcal{X} \rightarrow \mathbb{R}$ are parameter-dependent functions and parameter-independent continuous bilinear/linear forms, respectively. Moreover, $\Theta_q^A(\mu) \in \mathcal{C}^1(\mathcal{D})$, $1 \leq q \leq Q^A$, and $\Theta_q^F(\mu) \in \mathcal{C}^1(\mathcal{D})$, $1 \leq q \leq Q^F$, and the \mathcal{A}_q , $q \leq q \leq Q^A$, are symmetric. We further assume that our problem is well posed for all $\mu \in \mathcal{D}$ [22], [25].

We note that the new ‘‘expanded’’ formulation is no longer coercive, however, our output – the energy release rate – is now ‘‘compliant.’’ The former is bad news; the latter is good news. However, the real merit of the expanded formulation is that we effectively eliminate the nonlinearity of the output which will in term permit us to develop much simpler, more efficient, and much sharper error bounds. It will be seen in the numerical results of Section V that the ‘‘expanded’’ formulation does indeed produce better results and in particular much *sharper* error estimators than the ‘‘classical’’ formulation [24].

C. Model Problem

We consider a linear elasticity problem corresponding to a plate with a circular hole from which emanate two cracks. We consider only one quarter of the original problem, due to the symmetry of the model about the centerlines.

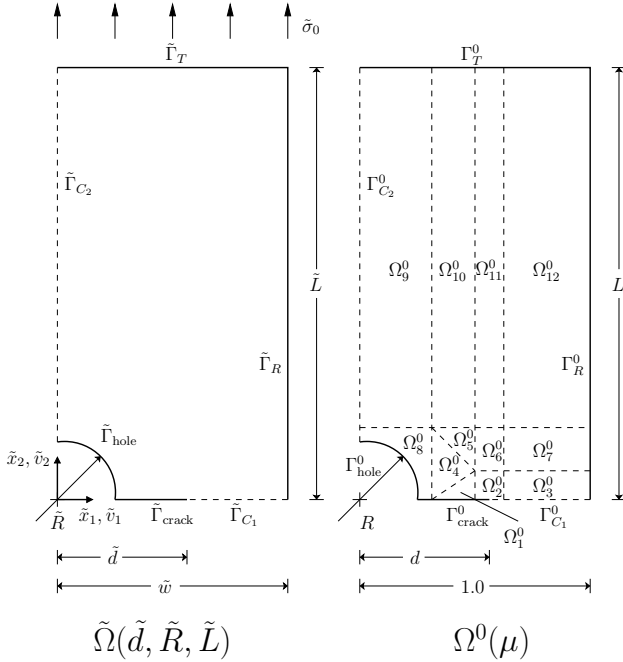


Fig. 1. Original dimensional domain (left); Non-dimensional domain (right)

We show in Figure 1 the resulting domain $\tilde{\Omega}^0(\tilde{d}, \tilde{R}, \tilde{L})$. The radius of the hole is \tilde{R} , the length of each side crack is \tilde{d} , and the plate is of width $2\tilde{w}$ and of length $2\tilde{L}$. We impose (normal) traction $\tilde{\sigma}_0$ at the top, $\tilde{\Gamma}_T$, zero traction on the hole, $\tilde{\Gamma}_{\text{hole}}$, zero traction on the crack, $\tilde{\Gamma}_{\text{crack}}$, zero traction on the right side of the plate, $\tilde{\Gamma}_R$, and symmetry boundary conditions on $\tilde{\Gamma}_{C_1}$ and $\tilde{\Gamma}_{C_2}$. We consider homogeneous isotropic material characterized by Young’s modulus \tilde{E} and Poisson ratio $\nu = 0.3$.

We choose for our characteristic length scale $\tilde{D} = \tilde{w}$ and denote our new non-dimensional domain and our boundaries correspond to $\tilde{\Omega}(\mu)$, and $\tilde{\Gamma}_{\text{hole}}, \tilde{\Gamma}_{\text{crack}}, \tilde{\Gamma}_{C_1}, \tilde{\Gamma}_{C_2}, \tilde{\Gamma}_T, \tilde{\Gamma}_R$ as $\Omega^0(\mu)$, and $\Gamma_{\text{hole}}^0, \Gamma_{\text{crack}}^0, \Gamma_{C_1}^0, \Gamma_{C_2}^0, \Gamma_T^0, \Gamma_R^0$, respectively.

In this example we shall consider $P = 3$ parameters: $\mu_1 \equiv d$ (the non-dimensional distance from the center of the hole to the crack tip), $\mu_2 \equiv R$ (the non-dimensional radius of the hole), and $\mu_3 \equiv L$ (the non-dimensional length of the specimen); our parameter domain is given by $\mathcal{D} = [0.325, 0.625] \times [0.1, 0.25] \times [1.5, 2.0]$. We choose $\bar{\mu} = (0.475, 0.175, 1.75)$ in the definition of our inner product.

The governing equation is the partial differential equations of linear elasticity: the displacement field $u^0(x; \mu) \in X^0$ satisfies

$$\int_{\Omega^0(\mu)} \frac{\partial u_i^0}{\partial x_j} C_{ijkl} \frac{\partial v_k}{\partial x_l} = \int_{\Gamma_T^0} v, \quad \forall v \in X, \quad (18)$$

where $C_{ijkl} = \bar{c}_1 \delta_{ij} \delta_{kl} + \bar{c}_2 (\delta_{ik} \delta_{jl} + \delta_{il} \delta_{jk})$ is the constitutive tensor. Here \bar{c}_1 and \bar{c}_2 are the Lamé constants for plain strain

$$\bar{c}_1 = \frac{\nu}{(1+\nu)(1-2\nu)}, \quad \bar{c}_2 = \frac{1}{2(1+\nu)}; \quad (19)$$

recall that $\nu = 0.3$ is the Poisson ratio. Note that $X^0 = \{(v_1, v_2) \in (H^1(\Omega))^2 | v_1|_{\Gamma_{C_2}^0} = 0, v_2|_{\Gamma_{C_1}^0} = 0\}$.

In order to apply our methodology we map $\Omega^0(\mu) \rightarrow \Omega \equiv \Omega^0(\mu = \mu_{\text{ref}} = (d_{\text{ref}} = 0.475, R_{\text{ref}} = 0.175, L_{\text{ref}} = 1.75))$: the mapping is piecewise-affine over the 12 subdomains, $\Omega_i^0 \rightarrow \Omega_i$, $i = 1, \dots, 12$. We refer to [22] for a completed mapping procedure and coefficient lists. The abstract statement for our classical formulation is then recovered for $Q^a = 24$, $Q^f = 4$. As a result, we also recover $Q^A = 40$ and $Q^F = 6$ for our expanded formulation.

III. FINITE ELEMENT METHOD

A. Extended finite element method

The characteristic property of elliptic linear PDEs, such as the linear elasticity problems of interest here, is that the solution $u(\mu)$ is smooth if the domain boundary Γ and load/source $f(\cdot; \mu)$ are smooth; in particular, if the domain boundary Γ is *not* smooth – as in fracture-mechanics crack problems – singularities can occur, with corresponding detriment to convergence rates. One way to overcome this difficulty is to effectively or actually include the relevant singularities in the finite element space. In this paper, we use the extended finite element method, which exploits the partition of unity property [8] to enrich the region around the crack tip with appropriate asymptotic fields. It is shown in [9] that the extended finite element method yields an optimal convergence rate of h^m (in the X norm) for elements of polynomial order m . Our extended finite element formulation is discussed in details in [22], here we only describe our results.

Our finite element approximation to the extended formulation is: given $\mu \in \mathcal{D}$, find (the ‘‘compliant’’ output)

$$\mathcal{G}_h(\mu) = \mathcal{F}_h(\mathcal{U}_h(\mu); \mu), \quad (20)$$

where $\mathcal{U}_h(\mu) \equiv (U_{+h}, U_{-h}) \in \mathcal{X}_h$ is our approximate solution to $\mathcal{U}(\mu) \equiv (U_+, U_-) \in \mathcal{X}$ and satisfies

$$\mathcal{A}_h(\mathcal{U}_h(\mu), \mathcal{V}; \mu) = \mathcal{F}_h(\mathcal{V}; \mu), \quad \forall \mathcal{V} \in \mathcal{X}_h; \quad (21)$$

here $\mathcal{X}_h \equiv X_h \times X_h$ where X_h is our enriched finite element approximation as described in [22]; \mathcal{A}_h and \mathcal{F}_h are defined as our numerical quadratures of the bilinear/linear forms \mathcal{A}_h and \mathcal{F}_h . We also denote by \mathcal{A}_{hq} , $1 \leq q \leq Q^A$, and \mathcal{F}_{hq} , $1 \leq q \leq Q^{\mathcal{F}}$ our numerical quadratures of the bilinear/linear forms associated with our affine parameter decompositions \mathcal{A}_q , $1 \leq q \leq Q^A$, and \mathcal{F}_q , $1 \leq q \leq Q^{\mathcal{F}}$, respectively.

B. Truth approximation

We shall build our reduced basis approximation upon, and measure the error in our reduced basis approximation relative to, a fixed “truth” finite element approximation \mathcal{U}_{h_t} – a surrogate for the exact solution, \mathcal{U} . In general, we must anticipate that $2\mathcal{N} = \dim(\mathcal{X}_{h_t})$ will be very large, and we must hence require that our reduced basis approach is mathematically and computationally stable as $\mathcal{N} \rightarrow \infty$.

We denote our truth approximation expanded space of dimension $2\mathcal{N}_t$ as $\mathcal{X}_{h_t} = X_{h_t} \times X_{h_t}$. We imbue \mathcal{X}_{h_t} with the inner product $(\mathcal{W}, \mathcal{V})_{\mathcal{X}_{h_t}} \equiv a_h(W_+, V_+; \bar{\mu}) + a_h(W_-, V_-; \bar{\mu}), \forall W = (W_+, W_-), V = (V_+, V_-) \in \mathcal{X}_{h_t}$, and induced norm $\|\mathcal{W}\|_{\mathcal{X}_{h_t}} = \sqrt{(\mathcal{W}, \mathcal{W})_{\mathcal{X}_{h_t}}}$. Then, given $\mu \in \mathcal{D}$, we find $\mathcal{U}_{h_t} \in \mathcal{X}_{h_t}$ such that

$$\mathcal{A}_{h_t}(\mathcal{U}_{h_t}, \mathcal{V}; \mu) = \mathcal{F}_{h_t}(\mathcal{V}; \mu), \quad \forall \mathcal{V} \in \mathcal{X}_{h_t}; \quad (22)$$

we can then evaluate the energy release rate as

$$\mathcal{G}_{h_t}(\mu) = \mathcal{F}_{h_t}(\mathcal{U}_{h_t}; \mu). \quad (23)$$

Finally, we define the truth inf-sup and continuity “constants” as

$$\beta_{h_t}(\mu) \equiv \inf_{\mathcal{W} \in \mathcal{X}_{h_t}} \sup_{\mathcal{V} \in \mathcal{X}_{h_t}} \frac{\mathcal{A}_{h_t}(\mathcal{W}, \mathcal{V}; \mu)}{\|\mathcal{W}\|_{\mathcal{X}_{h_t}} \|\mathcal{V}\|_{\mathcal{X}_{h_t}}}, \quad (24)$$

and

$$\gamma_{h_t}(\mu) \equiv \sup_{\mathcal{W} \in \mathcal{X}_{h_t}} \sup_{\mathcal{V} \in \mathcal{X}_{h_t}} \frac{\mathcal{A}_{h_t}(\mathcal{W}, \mathcal{V}; \mu)}{\|\mathcal{W}\|_{\mathcal{X}_{h_t}} \|\mathcal{V}\|_{\mathcal{X}_{h_t}}}, \quad (25)$$

respectively.

C. Numerical results

For this Mode I fracture model, the stress intensity factor can again be extracted from the energy release rate via (9). Furthermore, the SIF values for this problem are available for selected values of $\mu_2 = R$ in the form of a graph and table generated by numerical pre-solution of the elasticity PDE by a boundary element method [12].

Our truth approximation space \mathcal{X}_{h_t} is of dimension $2\mathcal{N}_t = 7,224$. The mesh is refined near the crack tip, and the enriched region is chosen as the first element ring around the crack tip (\mathcal{I}_M contains $M = 27$ nodes). We present our results in the form of a “boundary correction factor” $F(d, R, L) = \frac{K(d, R, L)}{\sqrt{d}} = \sqrt{\frac{G(d, R, L)}{d(1-\nu^2)}}$, and associated finite element approximation $F_h(d, R, L)$ (for the particular case $\nu = 0.3$); for purposes of presentation, we fix $L = 2.0$. We observe in Figure 2 that our finite element results are in good agreement with the reference results (only) available for $R = 0.1$ and $R = 0.25$.

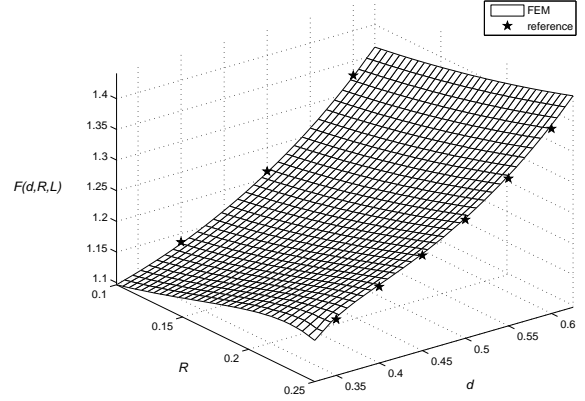


Fig. 2. Example 3.3: Boundary correction factor results for $L = 2.0$.

IV. REDUCED BASIS APPROXIMATION

In this Section we shall develop the reduced basis approximation for our expanded formulation – a non-coercive symmetric elliptic PDE with “compliant” output. As already indicated, the reduced basis is constructed not as an approximation to the exact solution $\mathcal{U}(\mu)$, but rather as an approximation to the finite element truth approximation $\mathcal{U}_{h_t}(\mu)$.

A. Approximation

We shall denote by $2N$ the dimension of the reduced basis approximation space; we shall denote by $2N_{\max}$ the upper limit on the dimension of the reduced basis space – N_{\max} determines the maximum reduced basis accuracy that can be achieved. We next introduce a set of nested samples in parameter space, $S_N = \{\mu_1 \in \mathcal{D}, \dots, \mu_N \in \mathcal{D}\}$, $1 \leq N \leq N_{\max}$, and an associated set of Lagrangian reduced basis approximation spaces $W_N = \text{span}\{(U_{h_t+}(\mu), 0), (0, U_{h_t-}(\mu)), 1 \leq n \leq N\}$, $1 \leq N \leq N_{\max}$; here $\mathcal{U}_{h_t}(\mu) = (U_{h_t-}(\mu), U_{h_t+}(\mu))(\mu)$ is the solutions to (22) for $\mu = \mu_n$. In actual practice we orthogonalize the snapshots with respect to the inner product $(\cdot, \cdot)_{\mathcal{X}_{h_t}}$ in order to preserve the good “conditioning” of the underlying PDE, or $W_N = \text{span}\{\zeta_m, 1 \leq m \leq 2N\}$, $1 \leq N \leq N_{\max}$, where the basis functions ζ_n (respectively, ζ_{n+N}) are generated from the $(\mathcal{U}_{h_t+}(\mu_n), 0)$ (respectively, $(0, \mathcal{U}_{h_t-}(\mu_n))$) by a Gram-Schmidt process with respect to the inner product $(\cdot, \cdot)_{\mathcal{X}_{h_t}}$. It is clear from the definition of W_N that the reduced basis space contains “snapshots” on the parametrically induced manifold $\mathcal{M}_{h_t} \equiv \{\mathcal{U}_{h_t}(\mu) | \mu \in \mathcal{D}\}$. We can anticipate that \mathcal{M}_{h_t} is very *low-dimensional* and *smooth*, and hence $\mathcal{U}_N(\mu) \rightarrow \mathcal{U}_{h_t}(\mu)$ (and $\mathcal{G}_N(\mu) \rightarrow \mathcal{G}_{h_t}(\mu)$) very rapidly; we should thus realize $N \ll \mathcal{N}_t$.

Our reduced basis approximation $\mathcal{U}_N(\mu)$ is then obtained by a standard Galerkin projection (for other options, see [15]): for any $\mu \in \mathcal{D}$, we find $\mathcal{U}_N(\mu) \in W_N$ such that

$$\mathcal{A}_{h_t}(\mathcal{U}_N(\mu), \mathcal{V}; \mu) = \mathcal{F}_{h_t}(\mathcal{V}; \mu), \quad \forall \mathcal{V} \in W_N; \quad (26)$$

the reduced basis approximation $\mathcal{G}_N(\mu)$ to $\mathcal{G}_{h_t}(\mu)$ can then be evaluated as

$$\mathcal{G}_N(\mu) = \mathcal{F}_{h_t}(\mathcal{U}_N(\mu); \mu). \quad (27)$$

B. Offline/Online computational procedure

As we have argued, it is plausible that in order to obtain an accurate reduced basis approximation $\mathcal{U}_N(\mu)$, the dimension of W_N , $2N$ can be quite small. However, since the elements of W_N are still “large” in some sense (the representation of ζ_n is of length $2\mathcal{N}_t$), the computational savings are not self-evident. In this section we develop an offline-online procedure that will enable us to evaluate our approximations in real-time.

To begin, we expand our reduced basis approximation as

$$\mathcal{U}_N(\mu) = \sum_{j=1}^{2N} \mathcal{U}_{N_j}(\mu) \zeta_j. \quad (28)$$

By choosing $\mathcal{V} = \zeta_i, i = 1, \dots, 2N$, in (26), it follows that the coefficients $\mathcal{U}_{N_j}(\mu)$ satisfy the $2N \times 2N$ linear algebraic system for $1 \leq i \leq 2N$

$$\sum_{j=1}^{2N} \left\{ \sum_{q=1}^{Q^A} \Theta_q^A(\mu) \mathcal{A}_{h_t q}(\zeta_j, \zeta_i) \right\} \mathcal{U}_{N_j}(\mu) = \sum_{q=1}^{Q^F} \Theta_q^F(\mu) \mathcal{F}_{h_t q}(\zeta_i); \quad (29)$$

this representation is a direct result of the affine decomposition of a and f . The reduced basis output can then be calculated as

$$\mathcal{G}_N(\mu) = \sum_{j=1}^{2N} \left\{ \sum_{q=1}^{Q^F} \Theta_q^F(\mu) \mathcal{F}^q(\zeta_j) \right\} \mathcal{U}_{N_j}(\mu). \quad (30)$$

The offline/online computational strategy is now clear.

In the *offline* stage – performed *once* – we first solve for the $\zeta_j, 1 \leq j \leq 2N_{\max}$; we then form and store $\mathcal{A}_{h_t q}(\zeta_i, \zeta_j), 1 \leq i, j \leq 2N_{\max}, 1 \leq q \leq Q^A$; and finally we form and store $\mathcal{F}_{h_t q}(\zeta_j), 1 \leq j \leq 2N_{\max}, 1 \leq q \leq Q^F$. Note all quantities computed in this stage are *independent* of the parameter μ and the spaces are “hierarchical” – we can extract from them any quantity for a particular $N \leq N_{\max}$. This stage requires $O(4Q^A N_{\max}^2 \mathcal{N}_t)$ operations and $O(4Q^A N_{\max}^2 + 4Q^F N_{\max})$ “permanent” storage. Note the operation count is dominated by the formation of the $\mathcal{A}_{h_t q}(\zeta_i, \zeta_j)$ inner products, once the ζ_j have been obtained; in the former we exploit the sparsity in the finite element stiffness matrix.

In the *online* stage – performed *many times*, for each new value of μ – we first assemble and solve the $2N \times 2N$ linear algebraic system (29) to obtain $\mathcal{U}_{N_j}, 1 \leq j \leq 2N$; we next perform the summation in (30) to obtain $\mathcal{G}_N(\mu)$. The operation count in this stage is $O(4Q^A N^2 + 2Q^F N)$ and $O(8N^3)$ to assemble and solve the linear algebraic system, respectively, and finally $O(4Q^F N^2)$ to evaluate the output. The essential point is that the complexity of the online stage is completely independent of \mathcal{N}_t ; since $N \ll \mathcal{N}_t$, we expect – in the online/deployed stage – significant computation savings relative to the classical direct approach. (Of course, the offline effort is considerable, and hence we must be in the many-query or real-time context to justify the reduced basis approach.)

C. Sample Construction

To construct our nested samples S_N and the associated reduced basis spaces W_N , we pursue a greedy algorithm: the strategy is rather heuristic, but in practice works very well. For a detailed discussion of the strategy, we refer to [22].

D. Numerical Results

The convergence rate for the reduced basis approximation $\mathcal{G}_N(\mu)$ is shown in Table I. The error E_N is the maximum of the relative error, $|\mathcal{G}_{h_t}(\mu) - \mathcal{G}_N(\mu)|/|\mathcal{G}_{h_t}(\mu)|$ over a random parameter test sample $\Xi_{\text{test}} \in \mathcal{D}$ of size $n_{\text{test}} = 3,000$. We observe very rapid convergence with N : even for this 3-parameter ($P = 3$) case, we need only $N = 30$ to obtain 10^{-4} accuracy. The computational savings is still very high (despite the large number of terms in our affine expansion): our online evaluation is about 10,000 times faster than the conventional evaluation; moreover, it is shown as in Table I that the reduced basis solution $\mathcal{G}_N(\mu)$ and the “truth” solution $\mathcal{G}_{h_t}(\mu)$ are indistinguishable for $N \geq 20$.

N	E_N	\mathcal{E}_N	$\bar{\eta}_N^{\mathcal{G}}$	Online Time	
				\mathcal{G}_N	$\Delta_N^{\mathcal{G}}$
5	1.04E-01	1.66E+02	37.19	1.80E-05	2.12E-03
10	6.01E-02	8.72E+01	30.67	2.32E-05	2.37E-03
20	9.08E-03	4.39E-01	41.86	5.95E-05	3.96E-03
30	2.36E-03	1.31E-01	53.17	1.92E-04	5.03E-03
35	9.42E-05	3.17E-02	51.40	2.12E-04	7.10E-03
40	4.58E-05	8.86E-03	42.42	2.78E-04	7.69E-03

TABLE I

REDUCED-BASIS ERROR, ERROR BOUND, EFFECTIVITY, AND ONLINE TIME TO EVALUATE $\mathcal{G}_N, \Delta_N^{\mathcal{G}}$, AS A FUNCTION OF N ; THE TIMING RESULTS ARE NORMALIZED WITH RESPECT TO THE TIME TO CALCULATE THE “TRUTH” OUTPUT \mathcal{G}_{h_t} .

V. A POSTERIORI ERROR ESTIMATION

In this section we shall discuss the development of a *posteriori* error estimators for reduced basis approximations. We require that the estimators are *inexpensive* – the online computational complexity is independent of \mathcal{N}_t ; *reliable* – an upper bound of the true error; and *sharp* – not overly conservative. We first discuss the construction of a lower bound for the inf-sup parameter $\beta_{h_t}(\mu)$; we then describe our *a posteriori* error estimation procedures for our problem.

A. Lower Bound for the Inf-Sup Parameter

Our error bound requires an inexpensive (online) and reasonably accurate lower bound $\beta_{LB}(\mu)$ for the “truth” inf-sup stability parameter $\beta_{h_t}(\mu)$. We construct our lower bound for the inf-sup parameter by the “natural norm” technique developed in [23]. The construction of the lower bound of $\beta_{LB}(\mu)$ is also decomposed into two stages: the offline stage – performed once, with computational cost depending on \mathcal{N}_t and usually *expensive*; and the online stage – performed many times, with the computational cost independent of \mathcal{N}_t and very *inexpensive*. We shall refer to the detailed procedure in [23].

B. Error bounds

We first define our error bound for the error in the output as

$$\Delta_N^{\mathcal{G}}(\mu) \equiv \frac{\varepsilon_N^2(\mu)}{\beta_{LB}(\mu)}, \quad (31)$$

where $\varepsilon_N(\mu)$ is the dual norm of the residual defined as $\varepsilon_N(\mu) = \sup_{\mathcal{V} \in \mathcal{X}_{h_t}} \frac{\mathcal{R}_{h_t}(\mathcal{V}; \mu)}{\|\mathcal{V}\|_{\mathcal{X}_{h_t}}}$ and $\mathcal{R}_{h_t}(\mathcal{V}; \mu) = \mathcal{F}_{h_t}(\mathcal{V}) - \mathcal{A}_{h_t}(\mathcal{U}_N(\mu), \mathcal{V}; \mu)$, $\forall \mathcal{V} \in \mathcal{X}_{h_t}$ is the residual associated with $\mathcal{U}_N(\mu)$.

We next define our the effectivity associated with our error bound for the output as

$$\eta_N^{\mathcal{G}}(\mu) \equiv \frac{\Delta_N^{\mathcal{G}}(\mu)}{|\mathcal{G}_{h_t}(\mu) - \mathcal{G}_N(\mu)|}. \quad (32)$$

It is show in [22], [25] that the output effectivity satisfies

$$\eta_N^{\mathcal{G}}(\mu) \geq 1, \quad \forall \mu \in \mathcal{D}; \quad (33)$$

equivalently, $\Delta_N^{\mathcal{G}}(\mu)$ is a rigorous upper bound for the error in our reduced basis output.

We also define our approximation of the (non-dimensional) stress intensity factor $K_N(\mu)$ and associated error bounds $\Delta_N^K(\mu)$ based on (9) as

$$K_N(\mu) = \frac{1}{2} \left\{ \sqrt{\mathcal{G}_N(\mu) - \Delta_N^{\mathcal{G}}(\mu)} + \sqrt{\mathcal{G}_N(\mu) + \Delta_N^{\mathcal{G}}(\mu)} \right\}, \quad (34)$$

$$\Delta_N^K(\mu) = \frac{1}{2} \left\{ \sqrt{\mathcal{G}_N(\mu) + \Delta_N^{\mathcal{G}}(\mu)} - \sqrt{\mathcal{G}_N(\mu) - \Delta_N^{\mathcal{G}}(\mu)} \right\}. \quad (35)$$

It readily follows [25] that

$$K_N(\mu) - \Delta_N^K(\mu) \leq K(\mu) \leq K_N(\mu) + \Delta_N^K(\mu), \quad \forall \mu \in \mathcal{D}. \quad (36)$$

These lower and in particular upper bounds for the SIF are extremely useful in applications that require *highly accurate* (and typically conservative) stress intensity factor evaluations such as Non-Destructive Evaluation (NDE), crack growth prediction, or brittle failure applications.

C. Offline/Online Computational Procedure

It remains to develop associated offline-online computational procedure for the evaluation of $\Delta_N^{\mathcal{G}}(\mu)$ and in particular $\varepsilon_N(\mu)$, the dual norm of the residual. We begin from our reduced basis approximation $\mathcal{U}_N(\mu) = \sum_{n=1}^{2N} \mathcal{U}_{Nn}(\mu) \zeta_n$ and affine decomposition to express the residual as

$$\begin{aligned} \mathcal{R}_{h_t}(\mathcal{V}; \mu) &= \sum_{q=1}^{Q^{\mathcal{F}}} \Theta_q^{\mathcal{F}}(\mu) \mathcal{F}_{h_t q}(\mathcal{V}) \\ &- \sum_{q=1}^{Q^{\mathcal{A}}} \sum_{n=1}^{2N} \Theta_q^{\mathcal{A}}(\mu) \mathcal{U}_{Nn}(\mu) \mathcal{A}_{h_t q}(\zeta_n, \mathcal{V}), \quad \forall \mathcal{V} \in \mathcal{X}_{h_t}. \end{aligned} \quad (37)$$

It is clear from linear superposition that we can express $\hat{e}_{h_t}(\mu) \in \mathcal{X}_{h_t}$ as

$$\hat{e}_{h_t}(\mu) = \sum_{q=1}^{Q^{\mathcal{F}}} \Theta_q^{\mathcal{F}}(\mu) \mathcal{C}_q + \sum_{q=1}^{Q^{\mathcal{A}}} \sum_{n=1}^{2N} \Theta_q^{\mathcal{A}}(\mu) \mathcal{U}_{Nn}(\mu) \mathcal{L}_{qn}, \quad (38)$$

where $(\mathcal{C}_q, \mathcal{V})_{\mathcal{X}_{h_t}} = \mathcal{F}_{h_t q}(\mathcal{V})$, $\forall \mathcal{V} \in \mathcal{X}_{h_t}$, $1 \leq q \leq Q^{\mathcal{F}}$, and $\mathcal{L}_{qn} = -\mathcal{A}_{h_t q}(\zeta_n, \mathcal{V})$, $\forall \mathcal{V} \in \mathcal{X}_{h_t}$, $1 \leq n \leq 2N$, $1 \leq q \leq Q^{\mathcal{A}}$; note that these problems are simple parameter-independent Poisson problems (albeit over a somewhat complicated enriched space).

It thus directly follows that

$$\begin{aligned} \|\hat{e}_{h_t}(\mu)\|_{\mathcal{X}_{h_t}}^2 &= \sum_{q=1}^{Q^{\mathcal{F}}} \sum_{q'=1}^{Q^{\mathcal{F}}} \Theta_q^{\mathcal{F}}(\mu) \Theta_{q'}^{\mathcal{F}}(\mu) (\mathcal{C}_q, \mathcal{C}_{q'})_{\mathcal{X}_{h_t}} \\ &+ 2 \sum_{q=1}^{Q^{\mathcal{F}}} \sum_{q'=1}^{Q^{\mathcal{A}}} \sum_{n=1}^{2N} \Theta_q^{\mathcal{F}}(\mu) \Theta_{q'}^{\mathcal{A}}(\mu) \mathcal{U}_{Nn}(\mu) (\mathcal{C}_q, \mathcal{L}_{q'n})_{\mathcal{X}_{h_t}} \\ &+ \sum_{q=1}^{Q^{\mathcal{A}}} \sum_{q'=1}^{Q^{\mathcal{A}}} \sum_{n=1}^{2N} \sum_{n'=1}^{2N} \Theta_q^{\mathcal{A}}(\mu) \Theta_{q'}^{\mathcal{A}}(\mu) \mathcal{U}_{Nn}(\mu) \mathcal{U}_{Nn'}(\mu) (\mathcal{L}_{qn}, \mathcal{L}_{q'n'})_{\mathcal{X}_{h_t}}, \end{aligned} \quad (39)$$

in terms of which we can then evaluate $\varepsilon_N(\mu) = \sqrt{\|\hat{e}_{h_t}(\mu)\|_{\mathcal{X}_{h_t}}^2}$. The expression (39) is simply a summation of products of parameter-dependent functions and parameter-independent inner products. The offline-online decomposition is now clear.

In the offline stage, we first solve for the quantities \mathcal{C}_q , $1 \leq q \leq Q^{\mathcal{F}}$; \mathcal{L}_{qn} , $1 \leq n \leq 2N_{\max}$, $1 \leq q \leq Q^{\mathcal{A}}$; we then perform and store the parameter-independent inner products, $(\mathcal{C}_q, \mathcal{C}_{q'})_{\mathcal{X}_{h_t}}$, $1 \leq q, q' \leq Q^{\mathcal{F}}$; $(\mathcal{C}_q, \mathcal{L}_{q'n})_{\mathcal{X}_{h_t}}$, $1 \leq n \leq 2N_{\max}$, $1 \leq q \leq Q^{\mathcal{F}}$, $1 \leq q' \leq Q^{\mathcal{A}}$; and $(\mathcal{L}_{qn}, \mathcal{L}_{q'n'})_{\mathcal{X}_{h_t}}$, $1 \leq n, n' \leq 2N_{\max}$, $1 \leq q, q' \leq Q^{\mathcal{A}}$. This requires $O(2N_{\max} Q^{\mathcal{A}} + Q^{\mathcal{F}})$ “truth” finite element Poisson solutions and $O(4N_{\max}^2 (Q^{\mathcal{A}})^2 + 2N_{\max} Q^{\mathcal{A}} Q^{\mathcal{F}} + (Q^{\mathcal{F}})^2)$ “ \mathcal{N}_t inner products.”

In the online stage, given a new parameter value μ , we simply evaluate the sum (39) in terms of $\Theta_q^{\mathcal{A}}(\mu)$, $\Theta_q^{\mathcal{F}}(\mu)$ and $\mathcal{U}_{Nn}(\mu)$ and the *pre-computed* parameter-independent inner products. The operation count for this stage is only $O(N^2(4Q^{\mathcal{A}})^2 + 2NQ^{\mathcal{A}}Q^{\mathcal{F}} + (Q^{\mathcal{F}})^2)$ – independent of \mathcal{N}_t . We do note that for our more complicated (affine) geometric mappings, $Q^{\mathcal{A}}$ can be quite large; we thus expect – due to the $(Q^{\mathcal{A}})^2$ scaling – that $\Delta_N^{\mathcal{G}}$ will be more expensive to evaluate (online) than \mathcal{G}_N ; we confirm this in the next section.

D. Numerical results

We present in Table I the error bounds and effectivities for Example 3.3 as a function of N . The error bound reported, \mathcal{E}_N , is the maximum of the relative error bound, $\Delta_N^{\mathcal{G}}(\mu)/|\mathcal{G}_{h_t}(\mu)|$, over the same test sample Ξ_{test} of Section IV.C. We denote by $\bar{\eta}_N^{\mathcal{G}}$ the average of the effectivity, $\eta_N^{\mathcal{G}}(\mu)$, over Ξ_{test} . We observe relatively good effectivity: our $\bar{\eta}_N^{\mathcal{G}}$ is usually of order $O(10 - 100)$.

It is seen that the computational savings are still very high: one online evaluation for an output and the associated error bound for $N = 30$ is about 80-100ms compared to approximately 9-12s for a “truth” solution; our online evaluation (even with error estimation) is still about 90-150 times faster than the classical approach. We also note from the timings that the cost of $\Delta_N^{\mathcal{G}}$ is significantly greater than the cost of \mathcal{G}_N : the reason it that $Q^{\mathcal{A}} = 40$ is relatively large for this problem due to the more complicated (affine) geometric mappings near the hole. As a result, the computational time for $\Delta_N^{\mathcal{G}}$ (which has dominant complexity order $O(4(Q^{\mathcal{A}})^2 N^2)$) is much greater than the computational time for \mathcal{G}_N (which is $O(8N^3)$) for small N .

VI. APPLICATIONS

In this section, we shall apply our results to a (rather simple) fracture analysis problem to demonstrate the advantage of our technique.

In the previous sections, we have constructed our reduced basis approximation to estimate stress intensity factors for the crack-hole problem. Our reduced basis approximation can estimate stress intensity factor and its associated error for an arbitrary (non-dimensional) parameter $\mu \in \mathcal{D}$, where $\mathcal{D} = [0.325, 0.625] \times [0.1, 0.25] \times [1.5, 2.0]$. For a given set of (dimensional) “input” $\tilde{\mu} \equiv (\tilde{d}, \tilde{R}, \tilde{L}, \tilde{w})$, we can estimate our stress intensity factor $\tilde{K}(\tilde{\mu})$ and its associated error $\Delta\tilde{K}(\tilde{\mu})$. We shall denote $\tilde{\mu}_1 \equiv \tilde{d}$ as our crack length parameter from now on to avoid any confusion.

A. Design analysis

The fatigue life of a component may be dominant determined by the propagation of crack. In many structure components contain small initial crack that does not cause failure at first, the crack, however, will develop under fatigue loadings until it eventually exceeds the tolerated length and causes failure. Thus, to ensure the structure component does not fracture, the crack must not be grow to a critical size during the design life of the component.

By applying fracture mechanics principles it is possible to predict the number of cycles spent in growing a crack to some specified length or to final failure. It is well-known that, assuming constant amplitude load fluctuation, the rate of crack growth in a specimen in the “stable growth” material region is given by Paris’s law [19]

$$\frac{d\tilde{\mu}_1}{dN_c} = C(\Delta\tilde{K}(\tilde{\mu}_1))^m, \quad (40)$$

where $\tilde{\mu}_1$ is the crack length, N_c is the number of cycles, $\Delta\tilde{K}(\tilde{\mu}_1)$ is the stress intensity fluctuation corresponds to the crack length $\tilde{\mu}_1$ and C, m are Paris’s constants. Paris’s constants are different for different materials and are determined by experiments. Assuming constant amplitude load fluctuation with constant stress range $\Delta\tilde{\sigma} = \tilde{\sigma}_{\max} - \tilde{\sigma}_{\min}$, the stress intensity factor fluctuation is given by $\Delta\tilde{K}(\tilde{\mu}_1) = \Delta\tilde{\sigma}\tilde{K}(\tilde{\mu}_1)$.

We now define our design scenario. We consider a crack-hole model corresponds to $\tilde{w} = 4.0$ (in.), $\tilde{L} = 8.0$ (in.) and $\tilde{R} = 0.8$ (in.). The material is A514 Martensitic steel, of which Paris’s constants are $C = 0.66 \times 10^{-8}$ and $m = 2.25$ and the critical stress intensity factor is $\tilde{K}_{1C} = 150$ (ksi $\sqrt{\text{in.}}$) [19]. We further assume that the minimum initial crack length is $\tilde{\mu}_1 = 1.4$ (in.), and the constant stress range is $\tilde{\sigma} \in [\tilde{\sigma}_{\min}, \tilde{\sigma}_{\max}] \equiv [25, 45]$ (ksi). We now need to estimate the design life of the component and the critical crack length.

The analysis will be separated into two steps. We shall first calculate the critical crack length $\tilde{\mu}_1^{\text{cr}}$ that would cause fracture. We then integrate the crack growth rate expression (40) between $\tilde{\mu}_1$ to $\tilde{\mu}_1^{\text{cr}}$ to obtain the design life of the component.

We calculate the critical crack length using a binary search algorithm. The critical crack length is defined as the crack length that would cause fracture, in particular, the corresponding stress intensity factor for $\tilde{\sigma}_{\max}$ will be equal to the material

critical stress intensity factor, $\tilde{K}(\tilde{\mu}_1^{\text{cr}}) = \tilde{K}_{1C}$ [19]. With the given data, we obtain $\tilde{\mu}_1^{\text{cr}} = 2.2514$ (in.) after 26 iterations, which corresponds to 28 reduced basis evaluations using $N = 40$ basis. Thanks to our *a posteriori* error estimation, by pursue another two binary searches for the upper bound/lower bound of the critical crack length [25], we can produce an error estimation for our calculation, $\tilde{\mu}_1^{\text{cr}} \in [2.2509, 2.2518]$, for our reduced basis approximation with $N = 40$ basis. The result show that our estimation is very accurate – the different between our result and the result using stress intensity factor calculations by direct finite element method is only of order $O(10^{-3})$, and approximately 100 times faster, as shown in the previous sections.

We then integrate the crack growth rate by a simple Euler integration scheme to obtain the design life of $N_{\text{cr}} = 15,694$ (cycles); the integration requires 160 stress intensity factor evaluations. Again, we can safely produce an error estimation for our calculation by constructing two separated integrations based on our critical crack length range that obtained earlier [25], the results are shown in Figure 3. It is observed that for $N = 30$ basis, the accuracy of our prediction is acceptable. For the case we use $N = 30$ basis, the computation involves 404 stress intensity factor evaluations and only takes less than one minute.

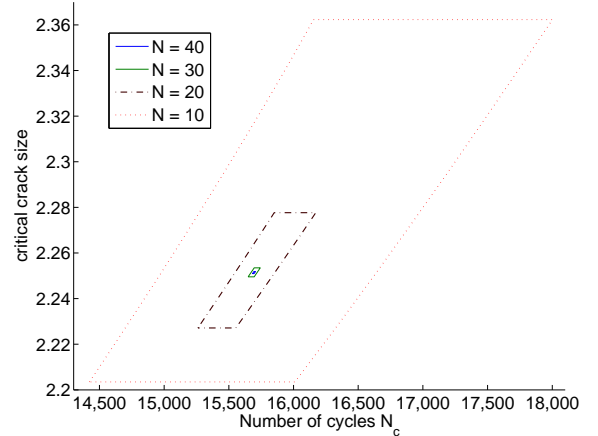


Fig. 3. Final design solution for different number of basis N in the reduced basis approximation.

We further assume the design life, N_{cr} , has to be larger, in particular, $N_{\text{cr}}^{\text{max}} = 20,000$ (cycles), thus the current design is inadequate. That requires us to modify our design parameter by changing the designed constant load stress range. We shall keep the maximum stress value and find the new minimum stress value that meet our new requirement. We again use the design analysis above as a “black box” and pursue another “outer” binary search, which we shall call our “black box” design analysis at each iteration. We finally obtained the new maximum constant stress range $\Delta\tilde{\sigma} = 18.025$ (ksi), or the new stress range is $\tilde{\sigma} \in [26.975, 45.000]$ (ksi) after 12 iterations, which only takes less than 11 minutes. This demonstrate that in many-query applications, our method works very efficiently.

B. Crack growth simulations

In practical, the stress range will rarely be the same to the designed parameter. In that case, fast crack growth simulation results would be very useful because it provides fast evaluation on the condition of the model. We conclude by providing several crack growth simulations for the final design parameter and different values of $\Delta\bar{\sigma}$, using $N = 15$ basis, in Figure 4. For each $\Delta\bar{\sigma}$ value, the simulation takes only around 15 seconds. We can conclude that our method can be used to provide very fast (or real-time) crack growth evaluations.

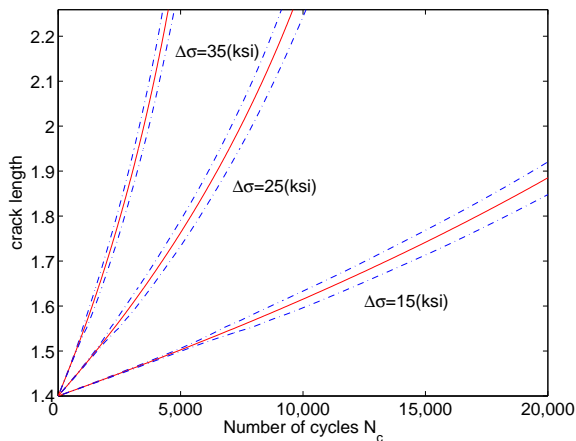


Fig. 4. Crack growth simulation results; the solid line is the predicted crack growth curve, the dash lines represent the error region of our calculations.

VII. CONCLUSIONS

We conclude that, our approach provides stress intensity factors at certified relative accuracy of 10^{-3} or 10^{-4} at less than $(1/100)^{\text{th}}$ the online cost of conventional numerical techniques. The savings would be even larger for problems with more complex geometry and solution structures, and in particular in higher space dimensions with correspondingly larger \mathcal{N}_t . We emphasize that the stress intensity factor/energy release rate is obtained very inexpensively but also reliably – thanks to the rigorous and relatively sharp *a posteriori* error bounds.

We also demonstrate the advantages of our technique by applying our results to a (rather simple) fracture applications. By using our technique, we are able to handle complex failure design analysis that requires many-query of stress intensity factor evaluations. It is also possible to produce several fracture parameter estimations in real-time using our approach. We conclude that applications in fracture mechanics which require either real-time computation (for example, Non-Destructive Evaluation or failure prediction) or many-query computation (fatigue crack growth prediction, say) of the stress intensity factor/energy release rate can benefit from our approach.

However, we emphasize that the method is *not* useful if only one (or a few) stress intensity factor evaluations are needed, due to the very expensive computational cost at the offline stage.

ACKNOWLEDGMENT

We would like to thank Professor David M. Parks of MIT, Professor David Clarke and Professor Anthony Evans of USCB for many helpful recommendations. This work was supported by DARPA and AFOSR under Grant F49620-03-1-0356 and the Singapore-MIT Alliance.

REFERENCES

- [1] D. M. Parks, *A stiffness derivative finite element technique for determination of crack tip stress intensity factors*, International Journal of Fracture 1974, **10**(4):487–502.
- [2] B. O. Amroth, P. Stern and F. A. Brogan, *Automatic choice of global shape functions in structural analysis*, AIAA Journal 1978, **16**:525–528.
- [3] A. K. Noor and J. M. Peters, *Reduced-basis technique for nonlinear analysis of structures*, AIAA Journal 1980, **18**(4):455–462.
- [4] J. P. Fink and W. C. Rheinboldt, *On the Error behavior of the Reduced Basis Technique for Nonlinear Finite Element Approximations*, Z. Angew. Math. Mech. 1983, **63**(1):21–28.
- [5] T. A. Porsching, *Estimation of the Error in the Reduced Basis Method Solution of Nonlinear Equations*, Mathematics of Computation, 1985, **172**:487–496.
- [6] M. D. Gunzburger, *Finite Element Methods for Viscous Incompressible Flows: A Guide to Theory, Practice, and Algorithms*, Academic Press (Boston), 1989.
- [7] J. S. Peterson, *The Reduced Basis Method for Incompressible Viscous Flow Calculations*, SIAM Journal of Scientific Computing, 1989, **10**(4):777–786.
- [8] I. Babuska, J. M. Melenk, *The partition of unity method*, International Journal for Numerical Methods in Engineering 1997, **40**:727–758.
- [9] G. Strang, G. J. Fix, *An analysis of the Finite Element Method*, Prentice-Hall, 1973.
- [10] C. Daux, N. Moës, J. Dolbow, N. Sukumar, T. Belytschko, *A finite element method for crack growth without remeshing*, International Journal for Numerical Methods in Engineering 1999, **46**:131–150.
- [11] M. B. Giles and N. A. Pierce, *Adjoint recovery of superconvergent functionals from PDE approximations*, SIAM Review 2000, **42**(2):247–264.
- [12] Y. Murakami, *Stress Intensity Factors Handbook*, Elsevier: 2001.
- [13] P. Heintz, F. Larsson, K. Hansbo and K. Runesson, *Adaptive strategies and error control for computing material forces in fracture mechanics*, Technical Report, Chalmers Finite Element Center, Chalmers University of Technology, Göteborg, Sweden, December 2002.
- [14] C. Prud'homme, D. Rovas, K. Veroy, Y. Maday and A. T. Patera, *Reliable real-time solution of parametrized partial differential equations: Reduced-basis output bound methods*, Journal of Fluids Engineering 2002, **124**(1):70–80.
- [15] Y. Maday, A. T. Patera, and D. V. Rovas, *A blackbox reduced-basis output bound method for noncoercive linear problems*, Nonlinear Partial Differential Equations and Their Applications, Collège de France Seminar Volume XIV, Elsevier Science B.V, 2002: 533–569.
- [16] S. S. Ravindran, *Adaptive Reduced-Order Controllers for a Thermal Flow System using Proper Orthogonal Decomposition*, SIAM Journal of Scientific Computing, 2002, **23**(6):1924–1942.
- [17] M. Barrault, N. C. Nguyen, Y. Maday, A. T. Patera, “An empirical interpolation” method: application to efficient reduced-basis discretization of partial differential equations, C. R. Acad. Sci. Paris, Serie I 2004, **339**:667–672.
- [18] T. L. Anderson, *Fracture Mechanics: Fundamentals and Applications*, 3rd edn, CRC, 2004.
- [19] J. M. Barsom, *Fracture and Fatigue Control in Structures*, 3rd edn, Butterworth-Heinemann, 2000.
- [20] N. C. Nguyen, K. Veroy and A. T. Patera, *Certified Real-Time Solution of Parametrized Partial Differential Equations*, Handbook of Materials Modeling, 1523–1558, Springer: 2005.
- [21] M. A. Grepl and A. T. Patera, *A Posteriori Error Bounds for Reduced-Basis Approximations of Parametrized Parabolic Partial Differential Equations*, M2AN. Mathematical Modelling and Numerical Analysis, 2005, **39**(1):157–181.
- [22] D. B. P. Huynh and A. T. Patera, *Reduced basis approximation and a posteriori error estimation for stress intensity factors*, International Journal For Numerical Methods In Engineering, 2006 (submitted).
- [23] S. Sugata, K. Veroy, D. B. P. Huynh, S. Deparis, N. C. Nguyen and A. T. Patera, *Natural Norm A Posteriori Error Estimators for Reduced Basis Approximations*, Journal of Computational Physics 2006, **217**(1):36–62.

- [24] D. B. P. Huynh, J. Peraire, A. T. Patera and G. R. Liu, *Real-Time Reliable Prediction of Linear-Elastic Mode-I Stress Intensity Factors for Failure Analysis*, SMA Symposium, 2006.
- [25] D. B. P. Huynh, *Reduced-Basis Approximation and Application to Fracture and Inverse Problems*, Ph.D Thesis, National University of Singapore, 2007.